J Mol Model (2011) 17:1149–1161
DOI 10.1007/s00894-010-0817-2

ORIGINAL PAPER

Docking and 3D-QSAR modeling of cyclin-dependent kinase 5/p25 inhibitors

Zaheer Ul Haq · Reaz Uddin · Lam Kok Wai · Abdul Wadood · Nordin Haji Lajis

Received: 4 March 2010 / Accepted: 19 July 2010 / Published online: 5 August 2010

Abstract Structure-based 3D-QSAR approaches (CoMFA and CoMSIA) were applied to understand the structural requirements of the Cyclin-dependent kinase 5/p25 inhibitors. Cyclin-dependent kinase 5 (CDK5) is believed to play an important role in the development of the central nervous system during the process of mammalian embryogenesis. Genetic algorithm based docking program (GOLD) was successfully utilized to orient the compounds inside the binding pocket of the CDK5/p25 structure. The adapted alignment method with the suitable parameters resulted in a reliable model. Furthermore, the final model was robust enough to forecast the activities of test compounds, satisfactorily. The contour maps were produced around the functional groups to understand the SAR requirements. Moreover, we also investigate the structural attributes of the inhibitors which make them selective toward CDK5/p25 over its close counterpart, i.e., CDK2. The study could be helpful to rationalize the new compounds with better inhibition and selectivity profiles against CDK5/p25.

Keywords CDK5/p25 · CoMFA · CoMSIA · Docking · 3D-QSAR

Z. Ul Haq (✉) · R. Uddin · A. Wadood
Dr. Panjwani Center for Molecular Medicine and Drug Research, International Center for Chemical and Biological Sciences, University of Karachi,
Karachi 75270, Pakistan
e-mail: zaheer.qasmi@iccs.edu

L. K. Wai · N. H. Lajis
Laboratory of Natural Products, Institute of Bioscience, University Putra Malaysia,
43400 UPM Serdang, Selangor Darul Ehsan, Malaysia

Introduction

Cyclin-dependent kinase 5 (CDK5) plays an essential role in the development of the central nervous system during mammalian embryogenesis. In the adult, CDK5 is required for the maintenance of neuronal architecture. Its deregulation has profound cytotoxic effects and has been implicated in the development of neurodegenerative diseases such as Alzheimer's disease and amyotrophic lateral sclerosis [1].

Cyclin-dependent kinase 5 (CDK5) is a member of a family of proline-directed serine/threonine kinases [1, 2]. It regulates a variety of processes in developing and adult neurons [3, 4]. CDK5 plays a central role in neuronal migration during the development of the central nervous system [4]. Additionally, p25 and p29 are equivalent proteolytic segments containing the *C*-terminal portion of p35 and p39, respectively. Excessive up regulation of CDK5 by the truncated activators contributes to neurodegeneration by altering the phosphorylation state of cytosolic and cytoskeletal proteins, and increased CDK5 activity has been implicated in Alzheimer's disease (AD), amyotrophic lateral sclerosis (ALS), Parkinson's disease, Niemann-Pick type *C* disease, and ischemia [5–9].

Postmortem brain analysis of AD patients reveals extensive formation of neurofibrillary tau protein tangles and amyloid plaques. The serine/threonine kinase CDK5 along with its cofactor p251 (or the longer cofactor, p35) has been supposed to hyperphosphorylate tau [10, 11], leading to the formation of paired helical filaments and deposition of cytotoxic neurofibrillary tangles [12] and thus responsible to neurodegenerative disorders such as Alzheimer's disease, Parkinson's disease, stroke, or Huntington's disease [13]. CDK5 also phosphorylates dopamine and Cyclic AMP-regulated phosphoprotein (DARPP-32) at threonine 75, indicating its role in dopaminergic neurotransmission [14].

Inhibition of the anomalous CDK5/p25 complex is, therefore, a viable target for treating Alzheimer's disease by preventing tau hyperphosphorylation and neurofibrillary tangle formation. Literature survey revealed 2-aminothienyl derivatives [3] as the potential inhibitors of CDK5/p25 for the treatment of Alzheimer's disease and other neurodegenerative disorders [15–21].

A number of CDK5/p25 inhibitors have been reported in the last couple of years [2, 22, 23]. Shiradkar et al. [11] reported a series of compounds exhibiting the potential to inhibit the CDK5/p25 complex. The aim of the study reported herein is to understand the SAR requirements in the inhibition mechanism of CDK5/p25 by a series of inhibitors reported by Shiradkar et al. [11]. In addition to that the current study is an attempt to understand the selectivity issue of the CDK5/p25 inhibitors with its close homologue of CDK2.

Over the last two decades, 3D-QSAR modeling including comparative molecular field analysis (CoMFA) and comparative molecular similarity indices analysis (CoMSIA) are emerged as reliable methods in order to understand the structural requirements of the ligands with respect to their receptors [24–27]. In the present study molecular docking method is utilized to orient the compounds in the binding site of CDK5/p25 and the top ranked conformations were subsequently used in the CoMFA model building.

Materials and methods

Molecular modeling

All molecular modeling methods were performed using Sybyl 7.3 on Genuine Intel ® Xeon ® 2.33 GHz Quadcore processor running under open SuSe Linux 11.0 environment.

Dataset

The compounds dataset and their inhibition profiles against the cyclin-dependent kinase 5/p25 (CDK5/p25) were collected from the literature reported by Shiradkar et al. [11]. Scheme 1a and b contains the structures and Table 1 includes the structures with their experimental inhibition constants (IC_{50}) in μM. Training and test set compounds were distributed randomly including 41 compounds in the training while the rest of the seven compounds were included in the test set. The IC_{50} values of the compounds were converted into their corresponding pIC_{50}s in order to utilize them in CoMFA PLS modeling.

Molecular docking and structural alignment

The 3D structures of all compounds were built and minimized using Sybyl 7.3 [28]. The geometries of all molecules were optimized by conjugate gradient's method using Tripos force field [29] with 1000 iterations. The AM1BCC charges [30] were calculated using the molcharge utility of the OpenEyes QuacPac [31]. Docking calculations were performed using GOLD program [32] with gold fitness score as the preferred scoring function. Default genetic operators of the GOLD docking program were used. Initially, the top ranked conformation of each compound was retrieved and subsequently utilized in CoMFA modeling. Then after, top ranked conformation of the most active compound was used as a template molecule in the database alignment method of Sybyl.

Setting up CoMFA and CoMSIA

The steric and electrostatic fields in CoMFA were calculated using an sp^3 carbon atom with +1.0 charge as the probe atom. Both electrostatic and steric field energies were truncated to ±30 kcal mol^{-1}. The CoMFA fields generated automatically and scaled by the CoMFA-STD method. In order to investigate the effect of grid spacing, initially the CoMFA models were developed at varying grid spacing values (*i.e.*, 0.5, 1.0 and 2.0: data not shown), and the best q^2 value was obtained when the grid spacing was set to the default 2.0 Å.

Another 3D-QSAR procedure, CoMSIA can avoid some inherent deficiencies arising from the functional forms of Lennard-Jones and Coulomb potentials used in CoMFA. In CoMSIA, a distance dependent Gaussian-type functional form has been introduced. This can avoid singularities at the atomic positions and the dramatic changes of potential energy due to grids in the proximity of the surface.

Similar to the usual CoMFA approach, a data table has been constructed from similarity indices [33] calculated via a common probe atom that is placed at the intersections of a regularly spaced lattice. A grid spacing of 2.0 Å has been used. Similarity indices $A_{F,\ K}$ between the compounds of interest and a probe atom, systematically placed at the intersections of the lattice, have been calculated according to the following equation (e.g., at grid point q for molecule j of the data set):

$$A^{q}{}_{F,K}(j) = -\sum_{i} \omega_{probe,k}\omega_{ik} e^{-\alpha r_{iq}{}^{2}}$$

Where i = summation index over all atoms of the molecule j under investigation; ω_{ik} = actual value of the physicochemical property k of atom i; $\omega_{probe,k}$ = probe atom with charge +1, α = attenuation factor; and r_{iq}=mutual distance between probe atom at grid point q and atom i of the test molecule. In the present study five physicochemical properties k (steric, electrostatic, hydrophobic and hydrogen bond donor and acceptor) were evaluated, using a common probe atom with 1 Å radius and charge, hydrophobicity and hydrogen-bond property of +1. Steric property fields were expressed by the third power of the atomic radii. The

Scheme 1 **a** Structures of the compounds from **1a**–**1b** to **9a**–**9 h. b** Structures of the compounds from **10a**–**10b** to **18a**–**18 h**

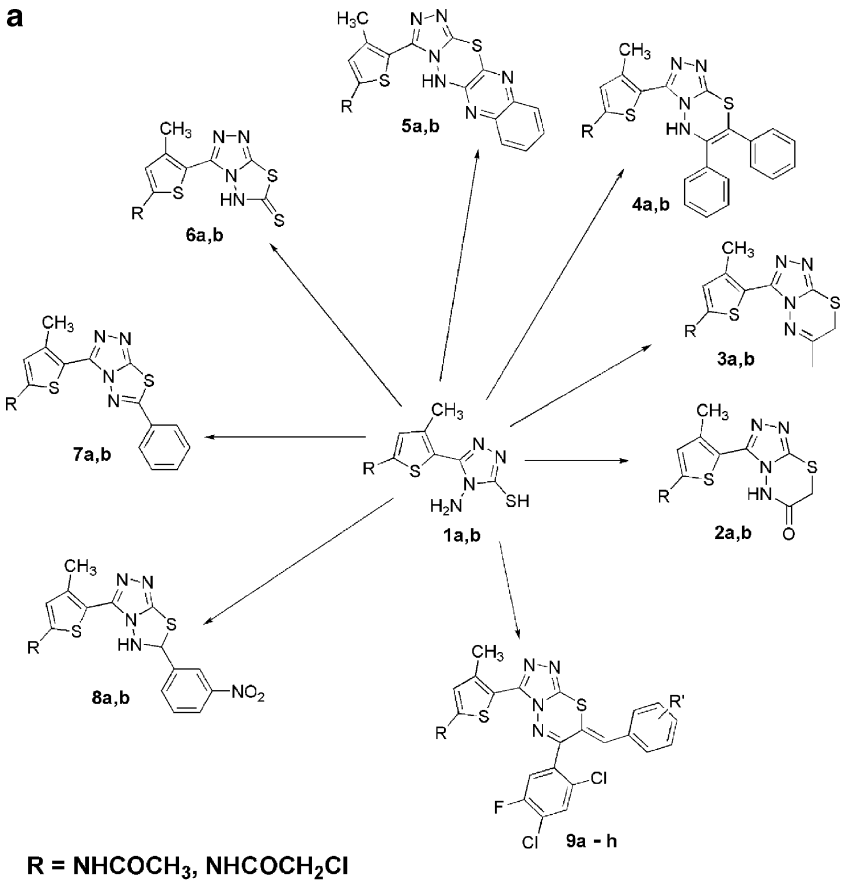

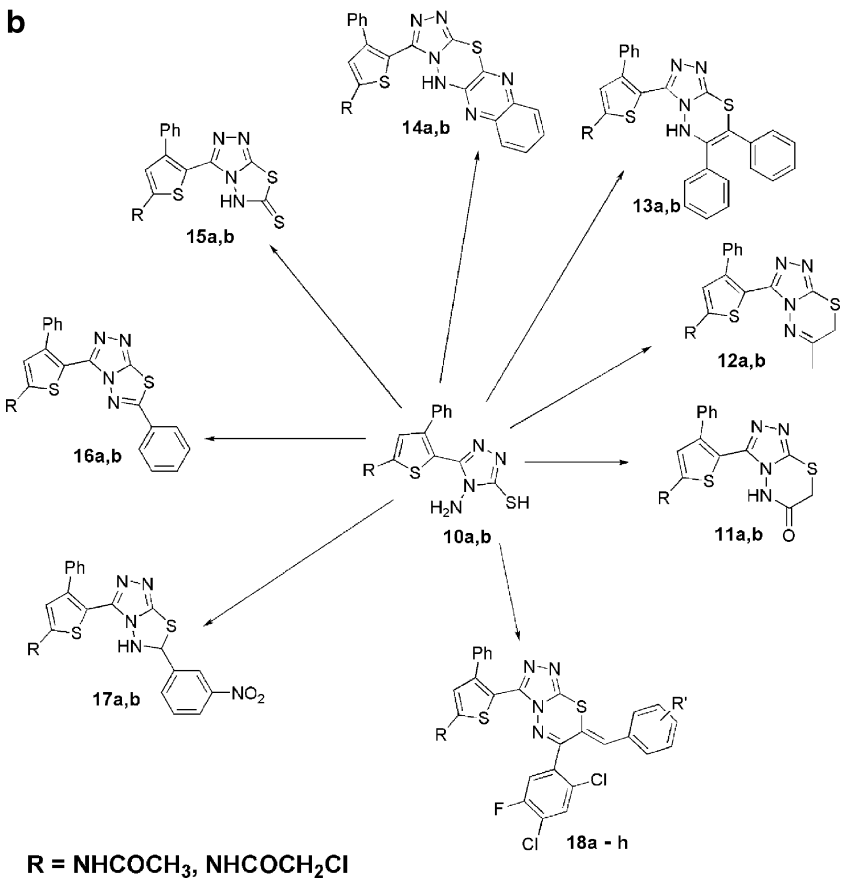

Table 1 Inhibitory activities (CDK5/p25) of the compounds. Their predicted pIC_{50}s and residuals were also reported by both CoMFA and CoMSIA models. (Parent skeletons could be found in Schemes 1a and b)

Compounds	R	R′	Experimental CDK5/p25 pIC_{50} (*n*M)	CoMFA predicted CDK5/p25 pIC_{50} (*n*M)	Residual	CoMSIA predicted CDK5/p25 pIC_{50} (*n*M)	Residual
1a	$NHCOCH_3$	—	7.24	7.12	0.12	7.22	0.02
1b	$NHCOCH_2Cl$	—	7.34	6.82	0.52	7.07	0.27
2a	$NHCOCH_3$	—	6.20	6.07	0.13	6.28	-0.08
2b [t]	$NHCOCH_2Cl$	—	6.09	6.14	-0.05	6.28	-0.19
3a	$NHCOCH_3$	—	6.19	6.15	0.04	6.27	-0.08
3b	$NHCOCH_2Cl$	—	6.34	6.41	-0.07	6.22	0.12
4a [t]	$NHCOCH_3$	—	7.36	7.03	0.33	7.31	0.05
4b	$NHCOCH_2Cl$	—	7.14	7.19	-0.05	7.36	-0.22
5a	$NHCOCH_3$	—	7.47	7.44	0.03	7.48	-0.01
5b	$NHCOCH_2Cl$	—	7.19	7.47	-0.28	7.26	-0.07
6a	$NHCOCH_3$	—	5.49	6.17	-0.68	5.57	-0.08
6b [t]	$NHCOCH_2Cl$	—	5.13	6.41	-1.28	5.76	-0.63
7a	$NHCOCH_3$	—	7.38	7.42	-0.04	7.22	0.16
7b	$NHCOCH_2Cl$	—	7.52	7.53	-0.01	7.33	0.19
8a [t]	$NHCOCH_3$	—	7.19	6.50	0.69	6.65	0.54
8b	$NHCOCH_2Cl$	—	7.28	7.02	0.26	7.17	0.11
9a	$NHCOCH_3$	H	5.63	5.56	0.07	5.58	0.05
9b	$NHCOCH_2Cl$	H	5.47	5.39	0.08	5.62	-0.15
9c	$NHCOCH_3$	2-Cl	5.48	5.53	-0.05	5.61	-0.13
9d	$NHCOCH_2Cl$	2-Cl	5.48	5.56	-0.08	5.56	-0.08
9e	$NHCOCH_3$	4-Cl	5.47	5.65	-0.18	5.45	0.02
9f	$NHCOCH_2Cl$	4-Cl	5.53	5.69	-0.16	5.46	0.07
9g	$NHCOCH_3$	3-NO_2	5.52	5.34	0.18	5.41	0.11
9h [t]	$NHCOCH_2Cl$	3-NO_2	5.51	5.45	0.06	5.49	0.02
10a	$NHCOCH_3$	—	7.27	7.20	0.07	7.46	-0.19
10b	$NHCOCH_2Cl$	—	7.38	7.30	0.08	7.29	0.09
11a	$NHCOCH_3$	—	6.38	5.88	0.51	6.24	0.14
11b	$NHCOCH_2Cl$	—	6.20	5.94	0.26	6.20	0.00
12a	$NHCOCH_3$	—	6.35	6.43	-0.08	6.39	-0.04
12b	$NHCOCH_2Cl$	—	6.43	6.47	-0.04	6.50	-0.07
13a	$NHCOCH_3$	—	7.40	7.25	0.16	7.34	0.06
13b	$NHCOCH_2Cl$	—	7.21	7.46	-0.25	7.37	-0.16
14a	$NHCOCH_3$	—	7.27	7.21	0.06	7.09	0.18
14b	$NHCOCH_2Cl$	—	7.52	7.49	0.03	7.63	-0.11
15a	$NHCOCH_3$	—	5.69	5.77	-0.08	5.39	0.30
15b	$NHCOCH_2Cl$	—	5.23	5.73	-0.50	5.39	-0.16
16a [t]	$NHCOCH_3$	—	7.42	7.09	0.33	7.21	0.21
16b	$NHCOCH_2Cl$	—	7.55	7.47	0.08	7.36	0.19
17a	$NHCOCH_3$	—	7.22	7.26	-0.04	7.25	-0.03
17b	$NHCOCH_2Cl$	—	7.32	7.45	-0.13	7.47	-0.15
18a	$NHCOCH_3$	H	5.84	5.84	0.00	6.12	-0.28
18b	$NHCOCH_2Cl$	H	5.6	5.21	0.39	5.59	0.01
18c	$NHCOCH_3$	2-Cl	5.61	5.72	-0.11	5.67	-0.06
18d	$NHCOCH_2Cl$	2-Cl	5.61	5.57	0.04	5.38	0.23
18e	$NHCOCH_3$	4-Cl	5.61	5.73	-0.12	5.56	0.05
18f	$NHCOCH_2Cl$	4-Cl	5.61	5.66	-0.05	5.76	-0.15

Table 1 (continued)

Compounds	R	R′	Experimental CDK5/p25 pIC_{50} (*n*M)	CoMFA predicted CDK5/p25 pIC_{50} (*n*M)	Residual	CoMSIA predicted CDK5/p25 pIC_{50} (*n*M)	Residual
18g [t]	$NHCOCH_3$	3-NO_2	5.61	5.66	-0.05	5.63	-0.02
18h	$NHCOCH_2Cl$	3-NO_2	5.57	5.66	-0.09	5.63	-0.06

Inhibition profile of the compound 16b with the CDK5/p25 = IC_{50} = 28±1 nM and against the CDK2 = IC_{50}=92±12 nM[11]

t = Test set compounds

CoMSIA results are interpreted graphically by field contribution maps using the field type "stdev*coeff".

Partial least squares (PLS)

The PLS method was used to set up a correlation between the molecular fields and the physicochemical property (dependent variable) of tested compounds. The optimal number of components was determined using cross-validation (leave-one-out) method. To speed up the analysis and reduce noise, columns with a value below 2.0 kcal mol^{-1} were filtered off. The cross-validated q^2 that resulted in optimum number of components and lowest standard error of prediction were taken. Then, final analysis was performed to calculate the conventional r^2 and standard error using the optimum number of components.

CoMFA/CoMSIA contour maps

Both CoMFA and CoMSIA contour maps were generated as a scalar product of coefficients and standard deviation (StDev*Coeff) associated with each column. Favored and disfavored levels, fixed at 80% and 20%, respectively. The steric fields are shown in green (more bulk favored) and yellow (less bulk favored), while the electrostatic field contours are displayed in red (electronegative substituents favored) and blue (electropositive substituents favored) colors.

In the CoMSIA (StDev*Coeff) hydrophobic contour plots, the favorable areas are indicated by yellow color, whereas the disfavored areas are shown by white color. Additionally, the contour plots of the CoMSIA H-bond donor and acceptor fields are presented. The favorable H-bond donor is shown in cyan while the less favorable donor areas are shown by purple contour. The favorable H-bond acceptor is shown in magenta, and the unfavorable H-bond acceptor is shown in red.

Results and discussion

CDK5/p25 and CDK2 comparison

The pdb structures of CDK5/p25 and CDK2 with the PDB IDs of 1UNG and 2WIH respectively, were downloaded. Both of the proteins were found as the dimer. In order to make a comparison, both structures were compared using the Matchmaker utility implemented in the program, Chimera [34]. The matched chains of both proteins were subsequently utilized. A sequence comparison between both proteins is given in Fig. 1. This sequence alignment revealed that both of the proteins are similar except for a little different active site residues. Difference in the residues at the active site could be the basis of selectivity toward CDK5/p25 of the studied compounds.

Molecular docking and structural alignment

In order to check the GOLD docking efficiency in reproducing the X-ray structure, the co-crystallized ligands of both the pdb files (1UNG; ALH and 2WIH; P48) were extracted and redocked using GOLD with default settings. The rmsds between the top ranked pose and the crystal structure were found consistent (1UNG; 1.35 Å and 2WIH; 1.47 Å), pointing out that the default GOLD settings are appropriate in order to carry out the inhibitors docking. In order to use the set GOLD docking parameters for the rest of the ligands docking simulations, a few of the CDK5 structures (PDB IDs: 1JSV, 1UNH and 1UNL) were retrieved from PDB. The re-docking experiments were performed with the co-crystallized ligands of these three CDK5 structures. A comparison between the docked and crystal ligand conformations of 1JSV, 1UNH and 1UNL resulted in the rmsds values of 1.50, 0.70 and 1.23 Å , respectively. The redocking experiments with these structures were also found satisfactory and in this way it allowed us to use the GOLD set parameters for docking simulations of ligands under study. In addition to self-docking, cross-docking simulations were also performed. The cross-docking simulations were conducted with the four CDK5 structures, i.e., 1UNG, 1JSV, 1UNH and 1UNL. The results of cross-docking were presented in Table 2. As expected the effectiveness of the applied docking protocol is decreased due to the slightly different conformations of the proteins in different crystallographic structures.

Figure 2 depicts ligand interactions of one of the most active compound (**16b**) when docked with both of the receptors (*i.e.*, CDK5/p25 and CDK2). Despite close

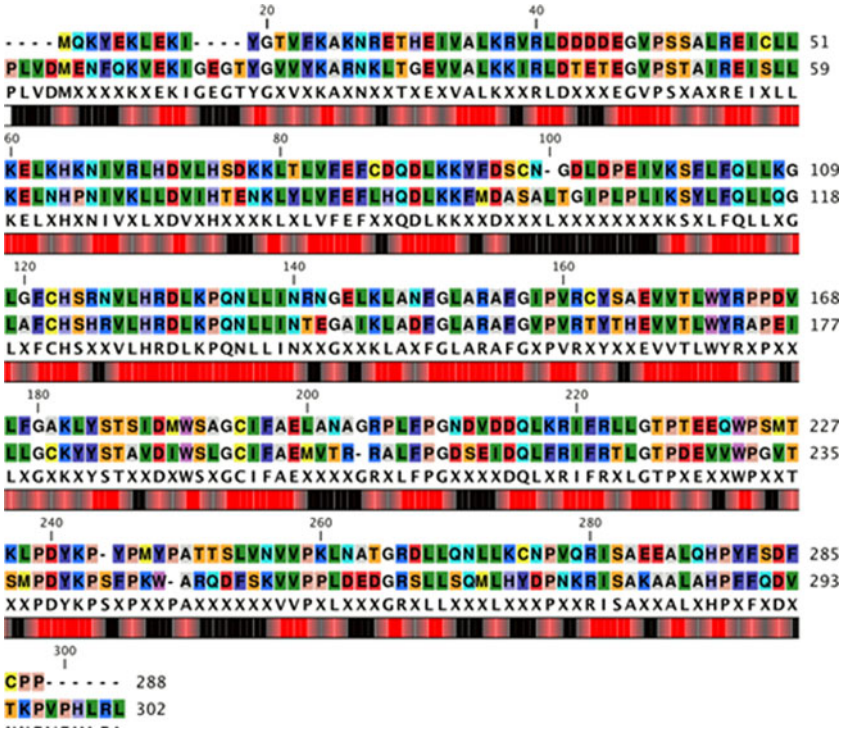

Fig. 1 Pair wise sequence alignment of 1UNG and 2WIH showing conserved residues in red while the non conserved residues are indicated as black. Consensus sequence is also shown at the bottom of aligned sequences. The above sequence is the CDK5/p25 and the bottom one is CDK2. The analysis is done using Chimera while image is generated by the program clcsequenceviewer [39]

similarities between the two receptors, Fig. 2a and b describe that the orientations of the compound's conformations in both of the receptors are totally independent. Particular emphasis should be on the role of the water molecule in the receptor 1UNG (Fig. 2a) which is mediating a strong hydrogen bond interaction with one of the pyrazole nitrogen atom. The interaction is observed when the compound is docked within the CDK5 receptor; therefore, this interaction is important in order to improve the selectivity profile of this class of compounds toward the CDK5.

To perform the structural alignments of the ligands, the top ranked docked solutions of each ligand was considered initially. The CoMFA requires a predefined hypothesis of the binding conformations of the compounds. Over the past two decades, molecular docking is established as a method of choice in recognizing the most probable bioactive conformation of the compounds with their corresponding receptors [35–38]. That's the reason we chose the docking method as alignment tool for the current study. This study hopes to shed some light on the efficiency of the docking method to be utilized as alignment tool for 3D-QSARs. Each ligand in the dataset was docked with both of the receptor structures using GOLD docking program. The subsequent top ranked conformations by GoldFitness scores were utilized in CoMFA modeling. The chosen top ranked docking solutions of each compound were well occupied in the binding sites and expected to be the best choice for CoMFA modeling. The selected top ranked conformation of each compound resulted in an acceptable model (modest q^2 value) but in terms of the external predictability, the model was not satisfactorily stable and failed to forecast the activities of test compounds accurately (data not shown). The inherent deficiency of the docking and then scoring is quite clear here and might be the main reason of poor performance of this model. It is well understood that the scoring functions are not able to rank the similar compound's docked conformations consistently. That's why, usually the superimpositions of the similar compounds, using the scoring as a primary criterion, are not guaranteed. Subsequently, the top ranked conformation of

Table 2 The rmsds (in Å) calculated during self-docking and cross-docking simulations

		Proteins →			
		1UNG	1JSV	1UNH	1UNL
↓ Ligands	1UNG	1.35	6.74	7.28	1.85
	1JSV	2.02	1.50	3.04	2.60
	1UNH	6.76	2.64	0.70	6.62
	1UNL	7.87	6.72	6.68	1.23

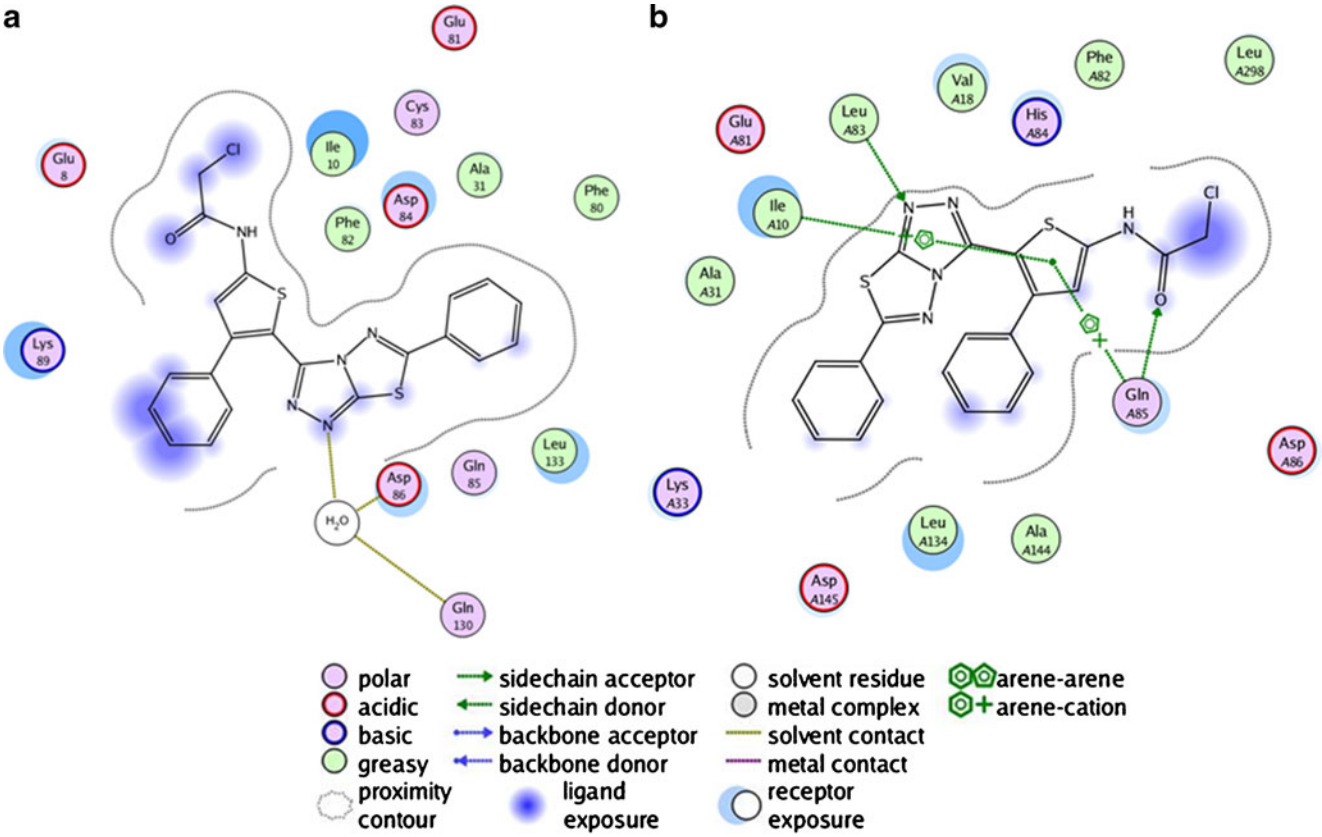

Fig. 2 The 2D depiction of the docked conformations of most active compound 16b within the binding sites of the receptors **a**) CDK5 (PDB: 1UNG) **b**) CDK2 (PDB: 2WIH). 2D depiction is rendered from MOE ligand interaction [40]

one of the most active compound (**16b**) was utilized as a template molecule in order to produce the appropriate aligned conformations of the rest of the ligands. This alignment method was found to produce improved results over the first method. The final aligned conformations of all the ligands are represented in Fig. 3. Scheme 2 is presented to describe overall scheme of the conformational sampling and CoMFA modeling.

CoMFA model

Forty-one of a total of forty-eight compounds were randomly selected as training set to develop the CoMFA model. The remaining seven compounds were used as test set for external validation of the CoMFA model. PLS analysis resulted in satisfactory q^2 and r^2 values, exhibiting the robustness of the selected model. Table 3 contains summary of the final PLS analysis. In the CoMFA model with the receptor CDK5/p25 (PDB ID: 1UNG), the leave-one-out cross-validated value q^2 was 0.737. On the other hand, the non-cross validated value r^2 was also satisfactory, *i.e.*, 0.930. The steric fields in both the cases were contributed more than the electrostatic fields. The applicability of CoMFA model was validated by predictions of the activities of the test compounds and found well correlated with predictive *r*-squared of 0.78. The predicted and experimental activities of training and test compounds with residuals by 1UNG model are reported in Table 1. The

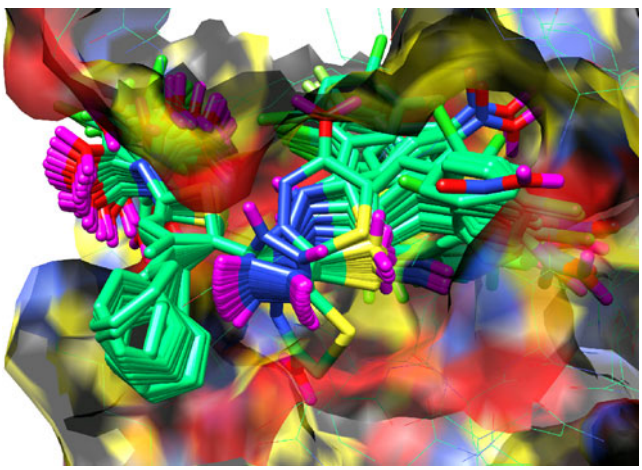

Fig. 3 Structural alignment of the compounds by database alignment method using top most docked conformation of compound **16b** as template. The aligned ligands are surrounded by the binding site of the receptor CDK5/p25 (PDB: 1UNG) and is rendered in surface. Hydrogen atoms are omitted for clarity purposes

Scheme 2 Overall scheme of the conformational sampling and CoMFA modeling

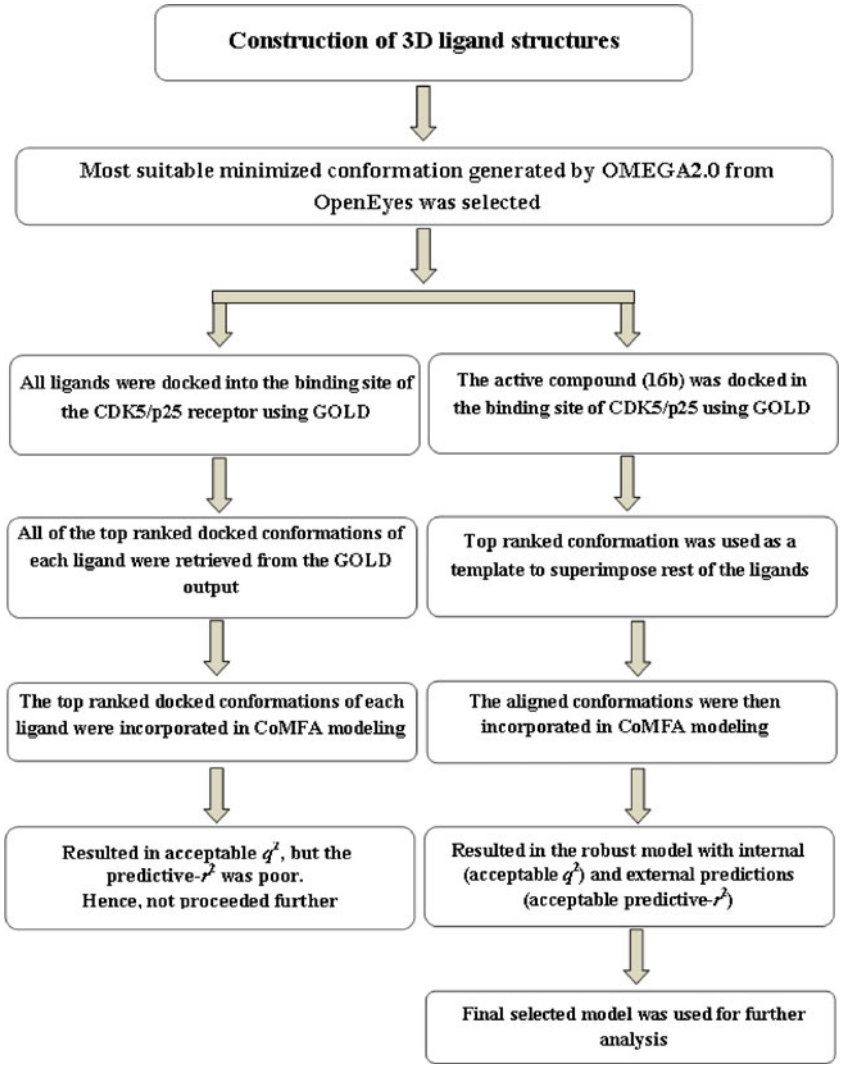

Table 3 Results of the CoMFA and CoMSIA analyses for the training and test set compounds

	CoMFA 1UNG	CoMSIA				
		S, E, H, D, A [(h)]	S, E [(h)]	S, E, H [(h)]	S, E, H, A [(h)]	S, E, H, D [(h)]
q^2 [a]	0.737	0.779	0.683	0.723	0.718	0.780
SEP [b]	0.455	0.424	0.508	0.467	0.479	0.422
No. of components [c]	5	6	6	5	6	6
r^2 [d]	0.930	0.972	0.914	0.918	0.927	0.972
SEE [e]	0.235	0.152	0.264	0.255	0.243	0.150
Field contributions	0.770, 0.230	0.190, 0.104, 0.392, 0.212, 0.101	0.613, 0.387	0.289, 0.178, 0.533	0.262, 0.162, 0.490, 0.086	0.220, 0.135, 0.406, 0.239
F-value [f]	93.287	193.916	60.238	78.185	72.223	198.591
Predictive *r*-squared [g]	0.78	0.95	0.81	0.78	0.81	0.93

[a] Cross-validated correlation coefficient. [b] Standard error of predictions. [c] Optimum number of components obtained from cross-validated PLS analysis and same used in final non-cross-validated analysis. [d] Noncross-validated correlation coefficient. [e] Standard error of estimate. [f] F-test value. [g] Correlation coefficient for test set predictions. [(h)] CoMFA and CoMSIA with different field contributions such as steric (S), electrostatic (E), hydrophobic (H), donor (D), and acceptor (A) fields

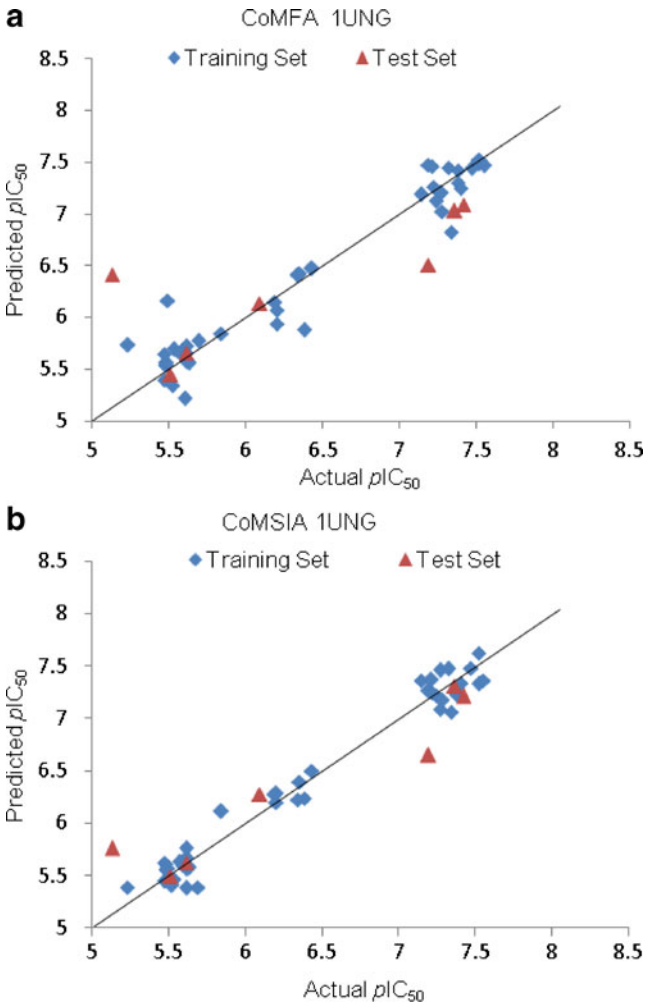

Fig. 4 Plots of predicted and actual activities of compounds by the models of **a**) CoMFA **b**) CoMSIA

correlation can be found in Fig. 4a. The collective information from Table 3 and Fig. 4a suggesting that a reliable CoMFA model is constructed. In order to further ascertain the statistical significance of the final selected model, an 18-fold cross-validation is performed. A comparison between the q^2 and predictive-r^2 with this cross-validation is presented as Fig. 5. The comparison revealed that the average q^2 and the predictive-r^2 values are significantly better and hence further confirms the robustness of the final selected CoMFA model.

CoMFA contour analysis

Figure 6 depicts the steric and electrostatic contour maps of CoMFA (StDev*Coeff) model. Template compound **16b** is presented as a reference compound in the Fig. 6. The favorable steric areas are indicated by green color, whereas the disfavored steric areas are shown by yellow color. The red contour represents that the electrostatically negative substituents can enhance the biological activity while the

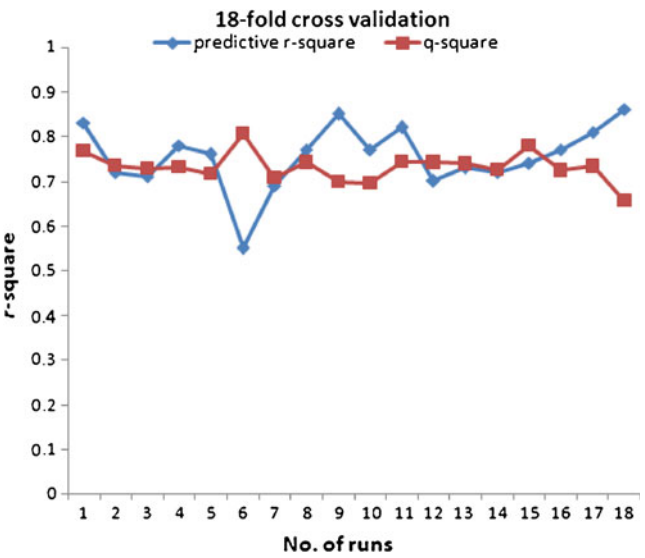

Fig 5 The comparison between the q^2 and the predictive-r^2 values over 18-fold cross validation

blue color represents that the increasing positive charge can enhance the biological activity at this region.

In Fig. 6 the green contour at near the phenyl ring of the compound **16b** is indicating that the sterically bulky group at the phenyl ring can increase the activity of the compounds.

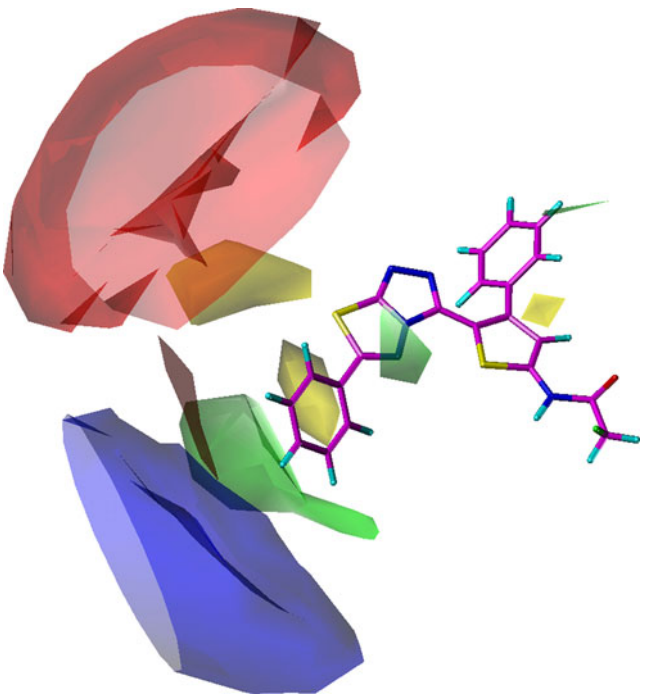

Fig. 6 Electrostatic and steric contour maps of CoMFA model. The docked conformation of compound **16b** (capped sticks in magenta) with the receptor CDK5/p25 (PDB: 1UNG) was shown inside the fields as reference molecule. The favorable steric areas with more bulk are indicated by green contours, whereas the disfavorable steric areas are shown by yellow contours. The favorable electrostatic areas with positive charges are indicated by blue contour, whereas the favorable electrostatic areas with negative charges are shown by red contour maps

This observation is consistent in the sense that the compounds **8a**, **8b**, **17a** and **17b** with the Nitro group (compared with the otherwise small H substituents at the same place) as the meta substituents are among the most active compounds in the series. Another green contour near the phenyl ring substituted on the thiophene ring is depicting the favorable interactions with the steric bulk. Hence the compounds bearing phenyl group substituted at the thiophene ring (*i.e.*, **16a**, **16b**, **17a**, **17b**, **14a** and **14b**) are relatively more active than their methyl substituted (*i.e.*, **7a**, **7b**, **8a**, **8b**, **5a** and **5b**) counterparts. Furthermore, the compounds pairs **4a**, **4b** and **13a**, **13b** bearing phenyl rings as sterically bulky substituents are among the active compounds. All these compounds have phenyl ring as the sterically bulky substituents in the same green contour region.

In Fig. 6 the yellow contour on the back side of the green contour is indicating that the compounds bearing big substituents near yellow contour are interacting badly and are detrimental to the steric complementarity and hence to the bioactivity. While examining the compounds **9a** to **9 h** and **18a** to **18 h**, it was observed that all these compounds are amongst the lowest active compounds in the series. When these compounds were placed in the contour maps, the substituents on the aromatic ring, attached with the thiadiazine ring, are approaching the yellow contours and hence they all are lowest active compounds.

In Table 3 the fraction of the steric and electrostatic field indicates the large contribution of steric fields and hence dominate the correlation with the biological activity. A large red colored contour beyond the yellow sterically disfavored region is indicating the non-co linearity of the electrostatically negative substituents with the receptor at this region. On the other hand, the blue colored contour map is indicating the favorable possibility to increase the electrostatically positive groups in order to enhance the biological activities. Unfortunately there are not many compounds present in the database which could come into contact with the electrostatic contour regions and that's why, the information about the requirements of electrostatic complementarity are quite limited. In order to investigate the electrostatic complementarity, another 3D-QSAR method named CoMSIA is performed. The details are in the following section.

CoMSIA model

PLS analysis with the CoMSIA descriptors resulted in satisfactory q^2 and r^2 values, exhibiting the robustness of the selected model. Table 3 contains summary of the final PLS analysis of CoMSIA model. In the CoMSIA model, the leave-one-out cross-validated value q^2 with combined steric (S), electrostatic (E), hydrophobic (H), hydrogen bond donor (D) and acceptor (A) fields was 0.779. On the other hand, the non-cross validated value r^2 with all five descriptors (SEHDA) was also satisfactory, *i.e.*, 0.972. The CoMSIA model was validated by predictions of the external test set compounds and a high predictive *r*-squared of 0.95 was found with all five CoMSIA descriptors. The predicted and experimental activities of training and test compounds with residuals by CoMSIA (SEHDA) model are reported in Table 1. The correlation can be found in Fig. 4b.

CoMSIA contour analysis

Figure 7 demonstrates the steric and electrostatic contour maps from CoMSIA model. The compound **16b** was presented as a reference compound. Comparing Fig. 6 with Fig. 7, the first observation depicts that over all CoMFA and CoMSIA models are showing the similar electrostatic and steric contour maps. One major breakthrough, however, in the case of CoMSIA is that the large electrostatic and steric contours from CoMFA models (Fig. 6) are now relatively small and mostly overlapped with the steric contours. Therefore, the interpretation of CoMSIA steric and electrostatic contour analysis go in a similar way and hence, represent the need of a sterically bulkly group on the phenyl ring attached to the thiadiazine ring. For example the compounds having large substituents in the shape of two phenyl rings attached to thiadiazine ring (e.g., **4b**) or large bulky group in the form of naphthalene ring are very active in the compound series. An overlapped blue contour is also present at the same position where this sterically favored green contour is present. Despite the presence of the electrostatically positive contour at this region the steric field is playing a major role in order to enhance the

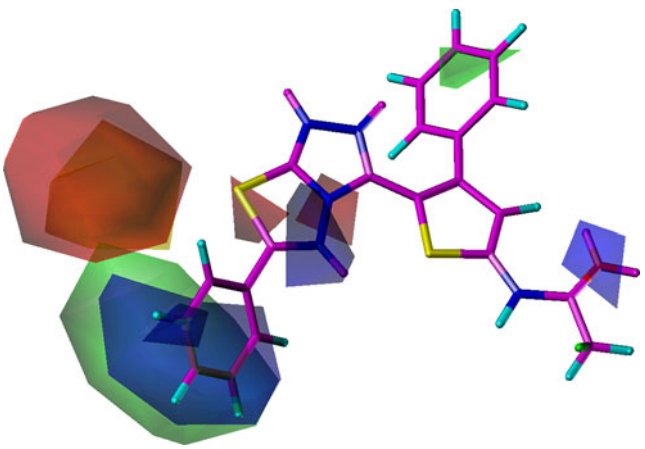

Fig. 7 Electrostatic and steric contour maps of CoMSIA model. The docked conformation of compound **16b** (capped sticks in magenta) with the receptor CDK5 (PDB: 1UNG), was shown inside the fields as reference molecule. The favorable steric areas with more bulk are indicated by green contours, whereas the disfavorable steric areas are shown by yellow contours. The favorable electrostatic areas with positive charges are indicated by blue contour, whereas the favorable electrostatic areas with negative charges are shown by red contour maps

biological activities. Alike of CoMFA, a similar steric disfavored region in the form of yellow contour is present which is supposed to interact badly with the large substituents present in the compounds from **9a** to **9 h** and **18a** to **18 h**. These compounds are the lowest actives in all series. In Table 3 the contribution of steric and electrostatic fields suggest that this is the steric complementarity which is playing a dominating role in describing the biological activity patterns within this compounds series. Another stericly favorable area is present at the phenyl ring which is attached to the thiophene ring and it behaves as a positive additive in terms of attaining the fair biological activity. For example small compound **10a** is not even able to accommodate the complete binding cavity of the enzyme but still is showing an observable amount of inhibition due to favorable interaction with its sterically bulky group near this region.

A very interesting observation is observed when we overlaid the CoMSIA hydrophobic contour maps with the most active compound **16b**. Figure 8 represents the CoMSIA hydrophobic fields with yellow contours as favorable hydrophobic area while white contour is disfavored hydrophobic area around the ligand. There is a large favorable hydrophobic region encompassing the whole of the substituents attached to the thiadiazine ring. A little distant from the large favorable area, there is a small unfavorable hydrophobic region represented by white contour present. A consistent trend is observed, when a compound bearing enough substituent limiting at the point of white contour is found poorly active (e.g., **3a**, **3b**, **12a** and **12b**) while the substituents which are larger enough to cross this disfavored region and touching the favorable region area are found most active in the series (e.g., **4a**, **4b**, **5a**, **5b** and so on). This observation is also consistent with the receptor binding site because of the fact that the residues of the receptor which are surrounding the substituents at thiadiazine ring are all non-polar or lipophilic in nature and hence creating a hydrophobic environment. The docking diagram in Fig. 2a is depicting this situation very clearly. Figure 9 represents the compound **16b** surrounded by the CoMFA steric and electrostatic contour maps while the interacting residues from the receptor are depicted in green. The interacting residues are clearly correlated with the docking identified interactions and the contour analysis.

The studied compounds are really not making significant hydrogen bonding interactions and hence the hydrogen bond descriptors are considered to be describing the minor SAR variations within the studied compounds. The statistics of CoMSIA models in Table 3 also suggest that the combination of steric (S), electrostatic (E) and hydrophobic (H) descriptors is in reality effecting significantly on the value of q^2 and hydrogen bond descriptors play no significant role. Therefore, the discussions of the contour maps generated with the CoMSIA hydrogen bond descriptors are omitted for current study.

Selectivity profile

The compounds studied here are active not only against CDK5/p25 but CDK2 as well (See the reference [11]). In order to understand the structural requirements which can make the derivatives more selective toward one on the

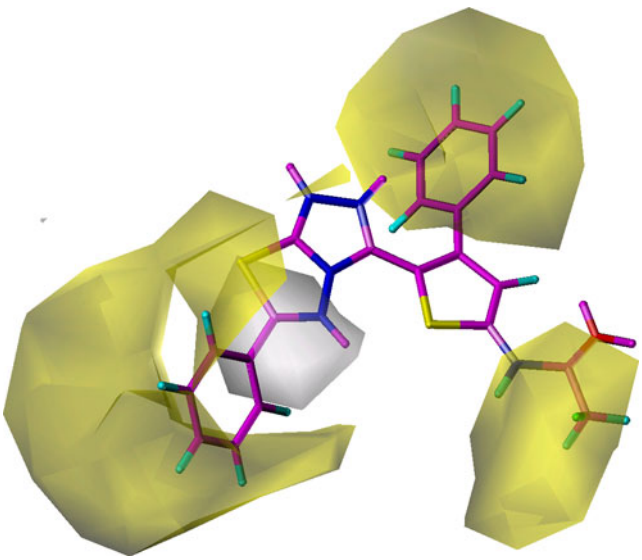

Fig. 8 Hydrophobic contour map from CoMSIA. The docked conformation of compound **16b** (capped sticks in magenta) with the receptor CDK5 (PDB: 1UNG), was shown inside the fields as reference molecule. The favorable hydrophobic areas are indicated by yellow contour, whereas the less favorable hydrophobic areas are shown by white contour maps

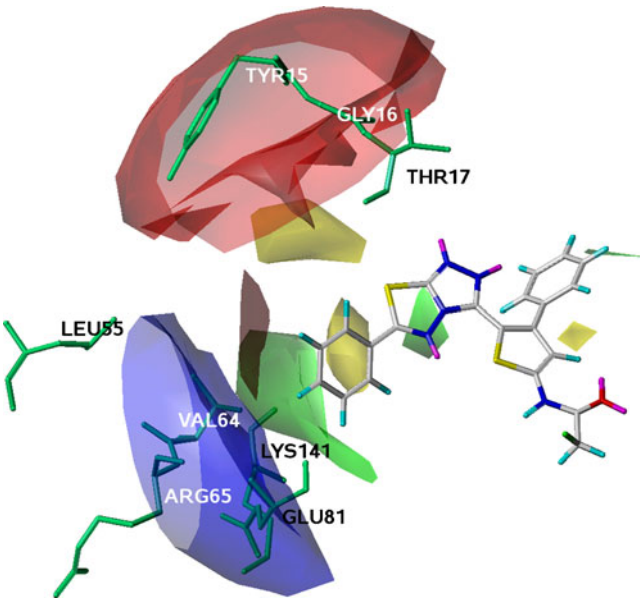

Fig. 9 The CoMFA contour map with the interacting residues from the receptor CDK5/p25. The docked conformation of compound **16b** (capped sticks in white) with the receptor CDK5/p25 (PDB: 1UNG) was shown inside the fields as reference molecule

other, we performed docking experiment of compound **16b** with the crystal structure of CDK2 (PDB ID: 2WIH) and overlaid the top docked conformation within the contour maps from both CoMFA and CoMSIA. As already clear that the steric requirements are playing the major role in the SAR of the compounds and CoMSIA steric contour maps are clear in explaining the structure requirements, that's why the CoMSIA steric contour maps were utilized in order to explain the selectivity requirements of the compounds.

Figure 10 shows the top ranked conformation of compound **16b** from both of the docking experiments, i.e., docked with receptor CDK2 (PDB ID: 2WIH) in white and with 1UNG in magenta; overlaid on the CoMSIA steric contour maps. Compound **16b**, which is three fold selective toward the CDK5/p25 (1UNG) protein (the activity of the compound **16b** against CDK2 given in the footnote of Table 1), is surrounded by CoMSIA steric and electrostatic contours. The analysis of Fig. 10 suggested that the conformation of compound **16b** from CDK2 docking (in white, Fig. 10) is interacting badly with the steric requirements at the yellow contour. Similarly, the same conformation is not satisfying the steric complementarity within the green contours. The other conformation in Fig. 10 which resulted when compound **16b** is docked with the CDK5/p25 (in magenta, Fig. 10), is favorably interacting with each steric contour map. This explains what is required to enhance the selectivity profile in order to optimize the existing compounds toward CDK5/p25 inhibitions. Although these two proteins are very similar but the contour analyses, depicted here, are giving insights in the details of the mechanism of how the same compounds are interacting with these two receptors. One can infer while comparing Fig. 10 and the docked 2D diagrams (Scheme**1**a and b) that the steric contour maps are well correlated with the binding sites since there are not many spaces available in the case of CDK5/p25 receptor at the phenyl ring substituted to the thiadiazole ring. Therefore, the compounds bearing the large substituents at this phenyl rings are relatively poor actives amongst all.

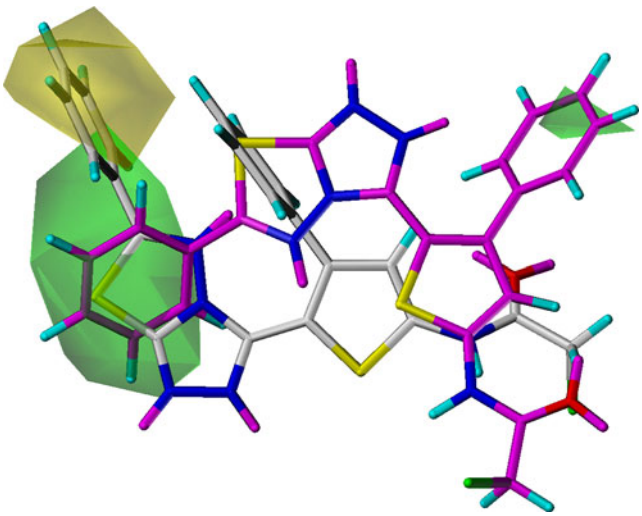

Fig. 10 The docked conformations of compound **16b** with the receptor CDK2 (capped sticks in white, PDB: 2WIH), and with the receptor CDK5/p25 (capped sticks in magenta, PDB: 1UNG) were shown inside the steric contour maps of the CoMSIA model

Conclusions

In order to develop a stable QSAR model to understand the structural requirements of the inhibitors with respect to their bioactivity profile enhancements against Cyclin-dependent kinase 5/p25 (CDK5/p25), molecular docking and 3D-QSAR modeling were carried out. Reliable 3D-QSAR models were developed with two methods (*i.e.*, CoMFA and CoMSIA). The obtained models were found satisfactory in terms of excellent internal (q^2>0.7) and external predictivity (predictive *r*-square>0.7). The top ranked docking conformation of the most active compound is utilized as a template in the step of conformational samplings. The docking analysis revealed the important interactions between the receptor active site residues and the compound's functional groups. Furthermore, the CoMFA and CoMSIA contour maps were produced and explained as per the biological enhancements. The contour maps were also correlated with the binding site environment and resulted in the observation that steric requirements are playing a major role in order to optimize the biological activities of the compounds. The CoMFA and CoMSIA contour analysis after correlating with the docked orientation of the compound **16b** suggested that there is still some space available with the case of receptor CDK2 but not in the case of CDK5/p25. This observation resulted in drawing the conclusion that the inhibition selectivity of the ligands could be achieved with the fine tuning of the steric complementarity of the region near the phenyl ring attached with the thiadiazine ring. Therefore, in general the sterically bulky substituents at this position are in favor of the CDK2 while the less sterically bulky group would be selective toward the CDK5/p25.

Additionally, the results reported here, demonstrated that the combined docking and 3D-QSAR approach is the best option in order to understand the binding orientation and then the functional requirements of the compounds in a hope to enhance the biological activities.

Acknowledgments Financial support from Higher Education Commission, Pakistan to Uddin, R., under the Split PhD program is highly acknowledged. Technical support by Prof. Bernd M. Rode, University of Innsbruck, Austria is highly acknowledged. Kok-Wai Lam acknowledged the financial support by the Ministry of Higher Education, Malaysia under the Fundamental Research Grant Scheme (FRGS) (01-11-08-651FR). Kok-Wai Lam was a recipient of Graduate Research Fellowship (GRF) scheme supported by UPM. The authors also acknowledge the Openeyes for providing the free academic license.

References

1. Mapelli M, Musacchio A (2003) The structural perspective on CDK5. Neurosignals 12:164–172
2. Mapelli M, Massimiliano L, Crovace C, Seeliger MA, Tsai LH, Meijer L, Musacchio A (2005) Mechanism of CDK5/p25 binding by CDK inhibitors. J Med Chem 48:671–679
3. Dhavan R, Tsai LH (2001) A decade of CDK5. Nat Rev Mol Cell Biol 2:749–759
4. Gupta A, Tsai LH (2003) Cyclin-dependent kinase 5 and neuronal migration in the neocortex. Neurosignals 12:173–179
5. Bu B, Li J, Davies P, Vincent I (2002) Deregulation of cdk5, hyperphosphorylation, and cytoskeletal pathology in the Niemann-Pick type C murine model. J Neurosci 22:6515–6525
6. Lau LF, Ahlijanian MK (2003) Role of cdk5 in the Pathogenesis of Alzheimer's Disease. Neurosignals 12:209–214
7. Nguyen MD, Julien JP (2003) Cyclin-dependent kinase 5 in amyotrophic lateral sclerosis. Neurosignals 12:215–220
8. Smith PD, Crocker SJ, Jackson-Lewis V, Jordan-Sciutto KL, Hayley S, Mount MP, O'Hare MJ, Callaghan S, Slack RS, Przedborski S (2003) Cyclin-dependent kinase 5 is a mediator of dopaminergic neuron loss in a mouse model of Parkinson's disease. Proc Natl Acad Sci USA 100:13650–13655
9. Wang J, Liu SH, Fu YP, Wang JH, Lu YM (2003) Cdk5 activation induces hippocampal CA1 cell death by directly phosphorylating NMDA receptors. Nat Neurosci 6:1039–1047
10. Hosoi T, Uchiyama M, Okumura E, Saito T, Ishiguro K, Uchida T, Okuyama A, Kishimoto T, Hisanaga S (1995) Evidence for cdk5 as a major activity phosphorylating tau protein in porcine brain extract. J Biochem 117:741–749
11. Shiradkar MR, Padhalingappa MB, Bhetalabhotala S, Akula KC, Tupe DA, Pinninti RR, Thummanagoti S (2007) A novel approach to cyclin-dependent kinase 5/p25 inhibitors: a potential treatment for Alzheimer's disease. Bioorg Med Chem 15:6397–6406
12. Lau LF, Seymour PA, Sanner MA, Schachter JB (2002) Cdk5 as a drug target for the treatment of Alzheimer's disease. J Mol Neurosci 19:267–273
13. Helal CJ, Sanner MA, Cooper CB, Gant T, Adam M, Lucas JC, Kang Z, Kupchinsky S, Ahlijanian MK, Tate B (2004) Discovery and SAR of 2-aminothiazole inhibitors of cyclin-dependent kinase 5/p25 as a potential treatment for Alzheimer's disease. Bioorg Med Chem Lett 14:5521–5525
14. Bibb JA, Snyder GL, Nishi A, Yan Z, Meijer L, Fienberg AA, Tsai LH, Kwon YT, Girault JA, Czernik AJ (1999) Phosphorylation of DARPP-32 by Cdk5 modulates dopamine signalling in neurons. Nature 402:669–671
15. Cooper CB, Helal CJ, Sanner MA (2002) EU Patent, EP1, 256, 578 A1
16. Kim KS, Kimball SD, Misra RN, Rawlins DB, Hunt JT, Xiao HY, Lu S, Qian L, Han WC, Shan W (2002) Discovery of aminothiazole inhibitors of cyclin-dependent kinase 2: synthesis, X-ray crystallographic analysis, and biological activities. J Med Chem 45:3905–3927
17. Misra RN, Xiao H, Kim KS, Lu S, Han WC, Barbosa SA, Hunt JT, Rawlins DB, Shan W, Ahmed SZ (2004) N-(cycloalkylamino) acyl-2-aminothiazole inhibitors of cyclin-dependent kinase 2. N-[5-[[[5-(1, 1-dimethylethyl)-2-oxazolyl] methyl] thio]-2-thiazolyl]-4-piperidinecarboxamide (BMS-387032), a highly efficacious and selective antitumor agent. J Med Chem 47: 1719–1728
18. Misra RN, Xiao H, Williams DK, Kim KS, Lu S, Keller KA, Mulheron JG, Batorsky R, Tokarski JS, Sack JS (2004) Synthesis and biological activity of N-aryl-2-aminothiazoles: potent pan inhibitors of cyclin-dependent kinases. Bioorg Med Chem Lett 14:2973–2977
19. Pevarello P, Amica R, Villa M, Salom B, Vulpetti A, Varasi M (2000) U.S. Patent 372,832
20. Pevarello P, Amici R, Traquandi G, Villa M, Vulpetti A, Isacchi A (2000) WO Patent 0026203
21. Sanner MA, Helal CJ, Cooper CB (2004) US Patent, U. S.6,720,427 B2.
22. Glicksman MA, Cuny GD, Liu M, Dobson B, Auerbach K, Stein RL, Kosik KS (2007) New Approaches to the Discovery of cdk5 Inhibitors. Curr Alzheimer Res 4:547–549
23. Leclerc S, Garnier M, Hoessel R, Marko D, Bibb JA, Snyder GL, Greengard P, Biernat J, Wu YZ, Mandelkow EM (2001) Indirubins inhibit glycogen synthase kinase-3 and CDK5/p25, two protein kinases involved in abnormal tau phosphorylation in Alzheimer's disease. J Biol Chem 276:251–260
24. Ravichandran V, Agrawal RK (2007) Predicting anti-HIV activity of PETT derivatives: CoMFA approach. Bioorg Med Chem Lett 17:2197–2202
25. Rodrigues CR, Flaherty TM, Springer C, McKerrow JH, Cohen FE (2002) CoMFA and HQSAR of acylhydrazide cruzain inhibitors. Bioorg Med Chem Lett 12:1537–1541
26. Zaheer-ul-Haq UR, Yuan H, Petukhov PA, Choudhary MI, Madura JD (2008) Receptor-based modeling and 3D-QSAR for a quantitative production of the butyrylcholinesterase inhibitors based on genetic algorithm. J Chem Inf Model 48:1092–1103
27. Zambre VP, Murumkar PR, Giridhar R, Yadav MR (2009) Structural investigations of acridine derivatives by CoMFA and CoMSIA reveal novel insight into their structures toward DNA G-quadruplex mediated telomerase inhibition and offer a highly predictive 3d-model for substituted acridines. J Chem Inf Model 49:1298–1311
28. Tripos (2003) Sybyl 7.3. Tripos Inc, St. Louis, MO
29. Clark M, Cramer Iii RD, Van Opdenbosch N (1989) Validation of the general purpose tripos 5.2 force field. J Comput Chem 10:982–1012
30. Jakalian A, Jack DB, Bayly CI (2002) Fast, efficient generation of high-quality atomic charges. AM1-BCC model: II. Parameterization and validation. J Comput Chem 23:1623–1641
31. QUACPAC (2008) version 1.3.1, Openeye scientific software, Inc, Santa Fe, NM, USA, www.eyesopen.com
32. Jones G, Willett P, Glen RC, Leach AR, Taylor R (1997) Development and validation of a genetic algorithm for flexible docking. J Mol Biol 267:727–748
33. Klebe G (1998) Comparative molecular similarity indices analysis: CoMSIA. Perspect Drug Discov Des 12:87–104
34. Huang CC, Couch GS, Pettersen EF, Ferrin TE (1996) In: Hunter L, Klein TE (eds) In Chimera: an extensible molecular modeling application constructed using standard components. Pacific Symposium on Biocomputing, Big Island, HI, January 3-6. World Scientific Publishing, Singapore, p 724
35. Akula N, Lecanu L, Greeson J, Papadopoulos V (2006) 3D QSAR studies of AChE inhibitors based on molecular docking scores and CoMFA. Bioorg Med Chem Lett 16:6277–6280
36. Chen H, Lyne PD, Giordanetto F, Lovell T, Li J (2006) On evaluating molecular-docking methods for pose prediction and enrichment factors. J Chem Inf Model 46:401–415
37. Radestock S, Bohm M, Gohlke H (2005) Improving binding mode predictions by docking into protein-specifically adapted potential fields. J Med Chem 48:5466–5479
38. Yu L, Yu PS, Yee Yen Mui E, McKelvie JC, Pham TPT, Yap YW, Wong WQ, Wu J, Deng W, Orner BP (2009) Phage display screening against a set of targets to establish peptide-based sugar mimetics and molecular docking to predict binding site. Bioorg Med Chem 17:4825–4832
39. CLC sequence viewer vers. 6.3 (CLC bio, Aarhus, Denmark)
40. Molecular Operating Environment MOE (2008)10, C. C. G. I. M., Quebec, Canada